# Modeling Shear Thickening in Dilute Polymer Solutions: Temperature, Concentration, and Molecular Weight Dependencies

**B. Jiang, D. J. Keffer, B. J. Edwards, J. N. Allred**

*Department of Chemical Engineering, The University of Tennessee, Knoxville, Tennessee 37996-2200*

Received 23 July 2002; accepted 7 April 2003

**ABSTRACT:** The Two Coupled Maxwell Modes (TCMM) Model is applied to give quantitative descriptions of shear-thickening behavior, which can be observed under certain conditions for high molecular weight polymers dissolved in low viscosity solvents. The TCMM Model is written in terms of five parameters representing the relaxation time of each mode, the concentration of each mode, and a coupling parameter between the two modes. Using all of the available experimental data for steady-shear viscosity and dichroism we found in the literature, we performed a full parameterization of these five quantities. Furthermore, from this parameterization we can describe the functional dependencies of the relaxation times, modal concentrations, and coupling parameter as functions of temperature, concentration, and molecular weight of the polymer. These functional dependencies are explained in light of the underlying physics imbedded in the TCMM Model. We demonstrate that by optimizing to only the viscosity data, we were able to obtain the same relaxation times, modal concentrations, and coupling parameter as using both the viscosity and dichroism data. This is useful because typically the experimental dichroism data is not available. © 2003 Wiley Periodicals, Inc. J Appl Polym Sci 90: 2997–3011, 2003

**Key words:** shear; solution properties; rheology; optics; phase separation

## INTRODUCTION

The anomaly of shear thickening, in which the viscosity of the solution increases with increasing shear rate, can be observed under certain conditions with high molecular weight polymers dissolved in low viscosity Newtonian solvents. Generally, dilute solutions of high molecular weight polymers dissolved in low viscosity Newtonian solvents display shear-thinning behavior, in which the viscosity of the solution decreases with increasing shear rate at intermediate and high shear rates.[1] However, shear thickening has been observed in some cases; the most recent literature review may be found in refs. 2 and 3. Although the shear-thinning phenomenon is regarded widely as an intramolecular effect due to the extension and orientation of the polymer chains in solution,[4] different explanations have been put forth to explain it.[5–11]

In Figure 1, we show a typical flow curve displaying shear thickening in a dilute polymer solution at a steady state. This experimental behavior of shear thickening was observed by Layec-Raphalen and Wolff[12] and Vraholpoulou and McHugh.[13] The usual pattern of shear-thinning behavior is evident at low to intermediate shear rates. The viscosity reaches a local minimum with increasing shear rate at $\dot{\gamma}_c$, and then the viscosity begins to increase with increasing shear rate. A local maximum in the viscosity is attained at a very high shear rate, $\dot{\gamma}_m$, followed by a resumption of shear thinning at extremely high shear rates.[12,13] At very low shear rates, not evident in Figure 1, the solutions presumably display a Newtonian plateau in viscosity relative to shear rate. However, as these solutions are very dilute, and hence their viscosities very low, linear viscoelastic behavior is not available because only high shear rate devices are experimentally manageable.

As mentioned above, the solutions under study are all dilute, meaning that the concentration of polymer in solvent is below the critical concentration for coil overlap, $c^*$.[2,3,12,13] Specific values of this quantity for the relevant solutions examined herein can be found in the references cited.

Various explanations of this anomalous behavior were reviewed in the preceding paper.[1] Some of these explanations are of intermolecular and some are of intramolecular origins.[5–11] Definitive experimental evidence confirming the intermolecular nature of shear thickening was provided in 1992 by Kishbaugh and McHugh.[2,3,14]

Rheo-optical measurements of linear dichroism, linear birefringence, and shear viscosity indicated that shear thickening was definitely associated with some

*Correspondence to:* B. Edwards (bjedwards@chem.engr.utk.edu).

Journal of Applied Polymer Science, Vol. 90, 2997–3011 (2003)

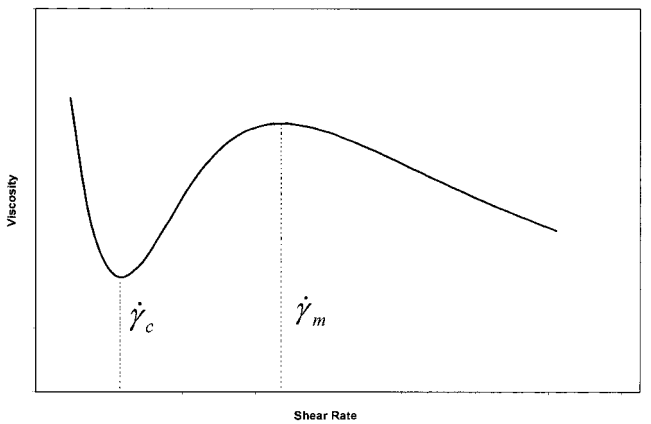


**Figure 1** A typical plot of viscosity versus shear rate for a dilute polymer solution that exhibits shear thickening. The increase in viscosity begins at the critical shear rate, $\dot{\gamma}_c$, and shear thinning resumes at $\dot{\gamma}_m$.

sort of supermolecular structure formation.[2,3,14] Typical experimental data from this study are illustrated in Figure 2. Note that almost concurrently with the critical shear rate, $\dot{\gamma}_c$, where the viscosity has a minimum, the linear dichroism displays a global maximum at $\dot{\gamma}_d$. The value of $\dot{\gamma}_d$ is usually equal to, or slightly less than, the value of $\dot{\gamma}_c$. At the same time, the magnitude of the linear birefringence increases monotonically with increasing shear rate.

Vrahopoulou and McHugh[13] advanced a conceptual basis for the shear-thickening behavior, and Kishbaugh and McHugh[2,3,14] extended it based on the rheo-optical data summarized in this paragraph and Figure 2. The main point of their explanation was that the solutions begin to develop micron-sized, optically-isotropic particles before the critical shear rate where the shear-thickening behavior begins to manifest, and that the continuous growth of these particles with increasing shear rate leads to the shear-thickening behavior evident in the viscosity curve.

There are some shortcomings to the explanation of shear thickening discussed above. First, it cannot explain why the onset of shear thickening always occurs at an equivalent or slightly larger value of shear rate than the maximum in the dichroism curve.[1] Second, there is a contradiction between the increase in size of the particles and the monotonic increase in birefringence with increasing shear rate.[1]

Edwards and coworkers[1] suggested a somewhat different explanation based on the Two Coupled Maxwell Modes (TCMM) Model.[1,15,16] In this explanation, at very low shear rates, the solutions exhibit a Newtonian plateau in viscosity, which is due to the short-time dynamics of the individual polymer chains and intermolecular associations. As shear rate increases, this plateau gives way to shear-thinning behavior, which is brought on by the stretching and orienting of the individual chains and the intermolecular structures. As the shear rate increases, the chains and structures continue to elongate and orient, and the viscosity of the solution continues to drop. At the critical shear rate, the viscosity of the solution is no longer able to support the extension of the structures, and subsequently they decrease in extension for higher shear rates. Once they have resumed a spherical distribution, they no longer contribute to changes in the relative stress level, and shear thinning resumes as the individual chain distribution continues to extend. This maximum in the extension of the structures with respect to shear rate rationalizes why the maximum in the dichroism curve always corresponds to the minimum in the viscosity curve. Moreover, these structures are not isotropic but anisotropic and are composed of anisotropic polymer chains, thus rationalizing the monotonically increasing behavior of the birefringence with increasing shear rate. The TCMM Model also predicts other rheological characteristic functions, such as the first and second normal-stress coefficients.

The experimental data in refs. 2, 3, 12, 13, 17, and 18 is generally not accurate enough near the viscosity minima to determine whether or not these minima are

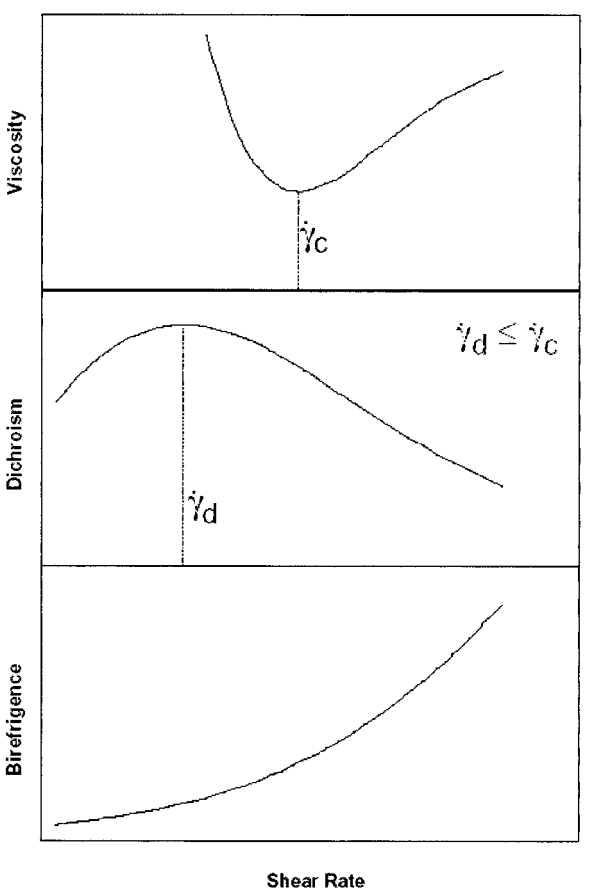


**Figure 2** Typical flow curves for viscosity, dichroism, and negative birefringence versus shear rate as observed in simultaneous rheo-optical measurements.

associated with a specific value of the shear stress. If such exists, the TCMM Model will also support this conclusion through the parameterized fits of the experimental data. However, without sufficiently accurate experimental data, no conclusions on this issue can be derived from the TCMM Model.

In the TCMM Model, there are five parameters: $\lambda_1$, $\lambda_2$, $n_1$, $n_2$ and $\theta$. The first two are the constant relaxation times of the two modes, measured in units of time. The first mode corresponds to the free polymer chains remaining in solution and the second to the supermolecular structures formed during shear. The second two parameters are the effective concentrations of the two modes, measured in units of moles per volume. The final (dimensionless) parameter, $\theta$, represents the degree of interaction between the two modes. Edwards and coworkers[1] applied the TCMM Model to a sampling of the experimental shear-thickening data available in the literature and used this to infer the physics behind this anomalous behavior, as described in the preceding paragraph. A sensitivity analysis therein[1] revealed the extent of uncertainties in the fitted values of these parameters.

In this paper, we present a full parameterization of the TCMM Model to all known experimental data from the literature. This provides a more thorough understanding of the significance of the model parameters, as well as insight into how they vary with concentration, temperature, molecular weight, and polymer architecture. Comparison of experimental data and model predictions results in a clearer insight into the peculiar behavior of shear thickening in dilute polymer solutions.

## Background

### The Two Coupled Maxwell Modes Model

The TCMM Model is a limiting case of the Multiple Coupled Modes Model, which was developed in ref. 15. In the TCMM Model, we use two conformation tensors, $\mathbf{c}^1(\mathbf{x}, t)$ and $\mathbf{c}^2(\mathbf{x}, t)$, to describe the orientation and extension of the individual polymer chains in solution and the supermolecular associations.[1] The eigenvalues and eigenvectors of these second-rank tensors quantify the extension and orientation of the two corresponding modes. The first conformation tensor, $\mathbf{c}^1(\mathbf{x}, t)$, is taken as the second moment of the distribution function, $\psi(\mathbf{x}, \mathbf{R}, t)$:[1,4]

$$\mathbf{c}^1 = \int \mathbf{RR}\psi d^3R. \tag{1}$$

In this expression, $\mathbf{R}$ is the end-to-end vector of a dissolved polymer chain. The second conformation tensor, $\mathbf{c}^2(\mathbf{x}, t)$, is associated with the intermolecular structures that form during shear and is given by

$$\mathbf{c}^2 = \int \mathbf{aa} f d^3a, \tag{2}$$

where $f(\mathbf{x}, \mathbf{a}, t)$ is the size distribution function of the structures and $\mathbf{a}$ is the vector spanning the major axis of an ellipsoidal structure.[1]

In the TCMM Model, these conformation tensors are not only affected by the applied deformation but by each other as well.[1,16] Many rheological models of differential type have been developed using uncoupled modes, in which the individual mode tensors are affected by the applied deformation only.[4] The introduction of coupling among the various modes of relaxation has led to a general class of coupled relaxation mode models derived in ref. 15. In the two Maxwell mode limit, the evolution equations for the conformation tensors are

$$\frac{\partial c^1_{\alpha\beta}}{\partial t} + v_\gamma \nabla_\gamma c^1_{\alpha\beta} - c^1_{\alpha\gamma}\nabla_\gamma v_\beta - c^1_{\beta\gamma}\nabla_\gamma v_\alpha = -\frac{1}{\lambda_1}c^1_{\alpha\beta} + \frac{k_BT}{\lambda_1 K_1}\delta_{\alpha\beta} - \frac{\theta}{2k_BT}\sqrt{\frac{n_2}{n_1}}\frac{1}{\sqrt{\lambda_1\lambda_2}} \times [K_2(c^1_{\alpha\gamma}c^2_{\beta\gamma} + c^2_{\alpha\gamma}c^1_{\beta\gamma}) - 2k_BTc^1_{\alpha\beta}],$$

$$\frac{\partial c^2_{\alpha\beta}}{\partial t} + v_\gamma \nabla_\gamma c^2_{\alpha\beta} - c^2_{\alpha\gamma}\nabla_\gamma v_\beta - c^2_{\beta\gamma}\nabla_\gamma v_\alpha = -\frac{1}{\lambda_2}c^2_{\alpha\beta} + \frac{k_BT}{\lambda_2 K_2}\delta_{\alpha\beta} - \frac{\theta}{2k_BT}\sqrt{\frac{n_2}{n_1}}\frac{1}{\sqrt{\lambda_1\lambda_2}} [K_1(c^2_{\alpha\gamma}c^1_{\beta\gamma} + c^1_{\alpha\gamma}c^2_{\beta\gamma}) - 2k_BTc^2_{\alpha\beta}]. \tag{3}$$

In these expressions, $k_B$ is Boltzmann's constant, $T$ is the absolute temperature, and $K_1$ and $K_2$ are the Hookean spring constants of each Maxwell mode. The parameters, $\lambda_1$, $\lambda_2$, $n_1$, and $n_2$ must be greater than or equal to zero for the model to make sense physically. The coupling parameter, $\theta$, appears to be lie within the range [0,1]; however, it is usually a small positive fraction.[16] Currently, there is no theory to provide values for these five parameters, and so they must be obtained from fits of the model to experimental data.

The extra stress tensor, $\sigma_{\alpha\beta}$, used for calculating the rheological properties of the polymer solutions, is a linear sum over the two conformation tensors,

$$\sigma_{\alpha\beta} = \sum_{i=1}^{2} (n_i N_A K_i c^i_{\alpha\beta} - n_i N_A k_B T \delta_{\alpha\beta}), \tag{4}$$

where $N_A$ is Avogadro's number. Using this expression, the rheological characteristic functions, such as the shear viscosity and normal stress coefficients, can be calculated in the usual fashion.[4] Note that the expressions in eq. (3) are easiest to solve in dimensionless form,[1] using dimensionless conformation tensors, $\tilde{\mathbf{c}}^i = K_i \mathbf{c}^i / k_B T$.

### Dichroism

Linear dichroism is the difference in intensity of linearly polarized light parallel and perpendicular to an axis of orientation.[17] This optical property is often used to obtain information about the size and shape of microstructural entities. The linear dichroism in our system is due to two sources, Rayleigh scattering from the structures and the innate dichroism of the individual molecules.[1,14] Consequently, the dichroism is expressed as $\Delta n'' = \Delta n''_1 + \Delta n''_2$, where

$$\Delta n''_1 = \frac{4\pi}{5} k^3 \frac{cN_A m_s}{M} (\alpha_1^2 - \alpha_2^2)_1 [\mathrm{tr}\, \tilde{\mathbf{c}}^1 - 3], \qquad (5)$$

and

$$\Delta n''_2 = \frac{8\pi}{15} m_p n_2 N_A k^3 (\alpha_1^2 - \alpha_2^2)_2 \frac{b}{(1 + 36/\sigma^2)}. \qquad (6)$$

The first term, eq. (5), is the innate dichroism of the deformed polymer chains. The symbols appearing in this equation are the wavenumber, $k = 2\pi/(6.328 \times 10^{-7}$ m), the polymer concentration, $c$ the polymer molecular weight, $M$, the refractive index of the solvent, $m_s = 1.474$, and the polarizability difference, $(\alpha_1^2 - \alpha_2^2)_1 = -1.25 \times 10^{-42}$ cm$^6$/molecule.[2,14]

The second term, eq. (6), is the linear dichroism of the supermolecular structures according to the Rayleigh Scattering Theory.[1,2,14] The symbols appearing in this expression are the refractive index of the polymer, $m_p = 1.59$, and several other functions. The anisotropy function, $b$, is given by

$$b = \frac{p^2 - 1}{p^2 + 1}, \qquad (7)$$

where $p$ is the sphericity or shape of the structure:[1]

$$p = (1 + \tfrac{3}{2}[\mathrm{tr}\, \tilde{\mathbf{c}}^2 - 3])^{3/4}. \qquad (8)$$

The quantity $\sigma$ is a dimensionless shear rate relative to the size and shape of the assumed structures:[2,14]

$$\sigma = \frac{\eta_s V_p v(p)}{k_b T} \dot{\gamma}, \qquad (9)$$

where $V_p$ is the volume of the structure,[1]

$$V_p = \frac{4\pi}{3p^2} a^3 = \frac{4\pi}{3p^2} ([\mathrm{tr}\, \tilde{\mathbf{c}}^2 - 3]\langle \mathbf{aa} \rangle_0)^{3/2}, \qquad (10)$$

and

$$\frac{1}{v(p)} = \frac{p^2}{p^4 + 1} \left[ -1 + \frac{2p^2 - 1}{2p\sqrt{p^2 - 1}} \ln \left[ \frac{p + \sqrt{p^2 - 1}}{p - \sqrt{p^2 - 1}} \right] \right]. \qquad (11)$$

In eq. (10), $\langle \mathbf{aa} \rangle_0$ is a parameter fitted to the dichroism curve by matching the maximum value of $\Delta n''$ at the shear rate $\dot{\gamma}_d$. After the parameter fitting has been completed, the effective structure size (length of major axis), $a$, can be determined by taking the square root of the primary eigenvalue of $\tilde{\mathbf{c}}^2$ multiplied by the factor $\langle \mathbf{aa} \rangle_0$: $a = \sqrt{(\lambda_p - 1)\langle \mathbf{aa} \rangle_0}$. The polarizability difference of the structures, $(\alpha_1^2 - \alpha_2^2)_2$, is given by

$$\frac{16\pi^2}{V_p^2} (\alpha_1^2 - \alpha_2^2)_2 = \left[ \frac{1}{L_1 + 1/(m_1^2 - 1)} \right]^2 - \left[ \frac{1}{(L_1 - 1)/2 + 1/(m_1^2 - 1)} \right]^2, \qquad (12)$$

where

$$L_1 = \frac{1 - e^2}{e^2} \left[ -1 + \frac{1}{2e} \ln \left[ \frac{1 + e}{1 - e} \right] \right]^2, \qquad (13)$$

and

$$e^2 = \left[ 1 - \frac{1}{p^2} \right]. \qquad (14)$$

Using these equations, the linear dichroism and its orientation angle relative to the direction of flow can be calculated after solving the TCMM Model for the non-vanishing components of $\tilde{\mathbf{c}}^1$ and $\tilde{\mathbf{c}}^2$.

## EXPERIMENTAL

The data that we used to obtain parameters for the TCMM Model were taken from refs. 2, 3, 12, 13, and 18. Layec-Raphalen and Wolff[12] measured viscosity as a function of shear rate for dilute solutions of Polystyrene/decalin (PS/d) of five different average molecular weights. Relative viscosities were measured with a capillary viscometer. They studied shear thickening for dilute solutions of PS/d as a function of concentration, molecular weight and shear rate, which yielded a quantitative analysis of the dependence of shear thickening on these variables.[12]

Vrahopoulou and McHugh studied shear thickening for three different polymer/solvent systems: polyethylene/xylene (PE/x), polypropylene/tetralin (PP/t), and polyethylene oxide/ethanol (PEO/e). They measured the viscosities of several crystallizable poly-

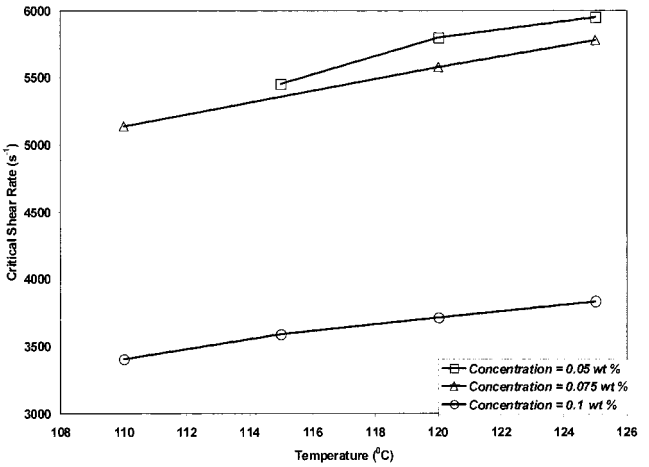


**Figure 3** Critical shear rates of PE/x ($M = 2.90 \times 10^6$ g/mole) solutions as function of temperature for $c = 0.05$, 0.075, 0.1 wt %.

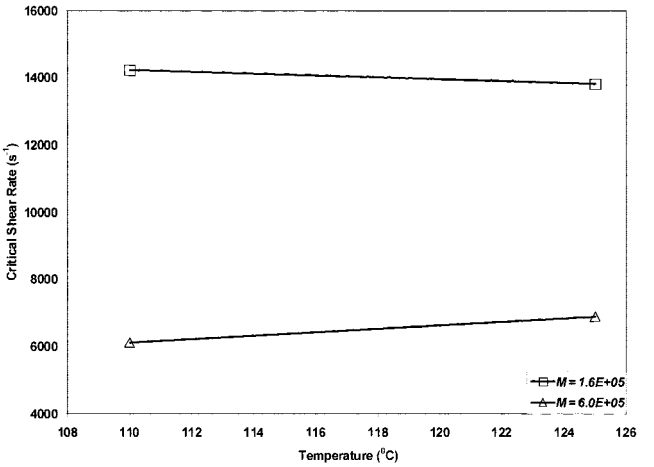


**Figure 5** Critical shear rates of PE/x solutions as functions of temperature for $M = 6.0 \times 10^5$, $1.6 \times 10^5$ g/mole.

mer solutions as functions of the wall shear rate in a capillary viscometer.

Kishbaugh and McHugh[2,3] obtained the most detailed experimental data on shear thickening by measuring not only the shear viscosity, but also the linear birefringence and linear dichroism and their associated orientation angles. A Couette flow cell was used in these simultaneous rheo-optical experiments to study the PS/d system.

The critical shear rate, $\dot{\gamma}_c$, where the minimum in the viscosity occurs, is a very important quantity for understanding shear thickening. From the available experimental data, we generated plots of the dependence of the critical shear rate on polymer concentration, temperature, and molecular weight. Results are presented in Figures 3, 4, and 5.

Figure 3 depicts $\dot{\gamma}_c$ for PE/x solutions as a function of temperature for three concentrations. We observe that the critical shear rate increases with increasing temperature for all concentrations. We can rationalize this behavior in terms of a physical mechanism: as the temperature increases, the viscosity of a liquid typically decreases. With lower viscosity, the shear thickening behavior is naturally postponed until higher shear rates are applied. One can also explain the increase in critical shear rate with increasing temperature by considering the temperature dependence of

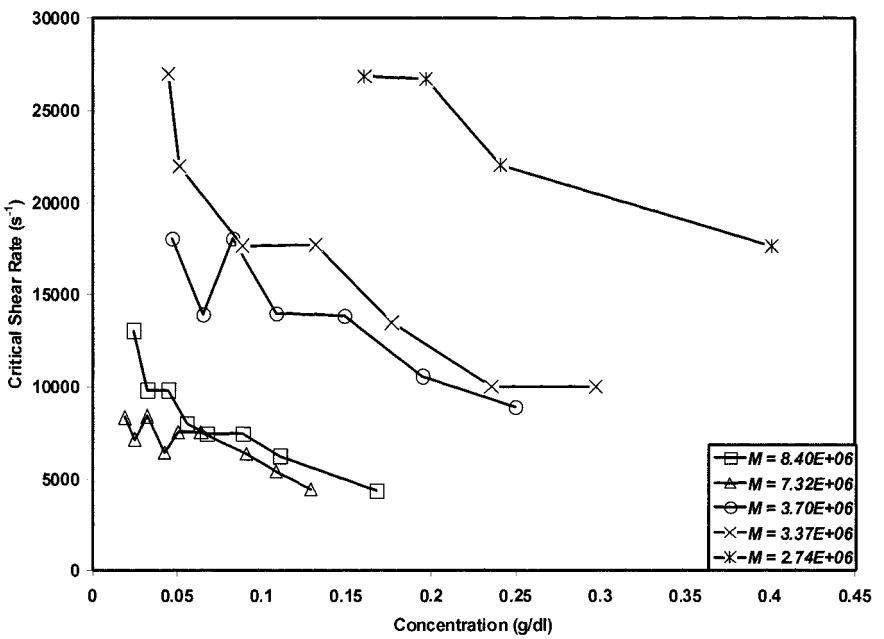


**Figure 4** Critical shear rates of PS/d solutions as functions of concentration for $M = 8.40 \times 10^6$, $7.32 \times 10^6$, $3.70 \times 10^6$, $3.37 \times 10^6$, $2.74 \times 10^6$ g/mole.

**TABLE I**
**Optimized parameters for PE/x Solutions of Vrahopoulou and McHugh[13,18]**

| $M$ (g/mole) | $T$ (°C) | $c$ (wt %) | $\lambda_1$ (s) | $\lambda_2$ (s) | $n_1$ (mole/m$^3$) | $n_2$ (mole/m$^3$) | $\theta$ (−) |
|---|---|---|---|---|---|---|---|
| 2.90E-06 | 110 | 0.0075 | 2.87E-03 | 7.41E-02 | 3.93E-05 | 1.74E-05 | 2.99E-03 |
| 2.90E-06 | 120 | 0.0075 | 2.62E-03 | 6.88E-02 | 3.85E-05 | 1.73E-05 | 3.04E-03 |
| 2.90E-06 | 125 | 0.0075 | 2.38E-03 | 7.60E-02 | 4.00E-05 | 1.85E-05 | 3.30E-03 |
| 1.6E-05 | 110 | 0.01 | 1.52E-03 | 3.07E-02 | 6.62E-05 | 3.00E-05 | 1.84E-03 |
| 1.6E-05 | 125 | 0.01 | 1.36E-03 | 3.09E-02 | 6.30E-05 | 2.88E-05 | 2.08E-03 |
| 6.0E-05 | 110 | 0.01 | 2.56E-03 | 6.70E-02 | 4.00E-05 | 1.94E-05 | 2.90E-03 |
| 6.0E-05 | 125 | 0.01 | 1.77E-03 | 5.72E-02 | 4.90E-05 | 2.36E-05 | 3.27E-03 |
| 2.90E-06 | 115 | 0.005 | 2.67E-03 | 8.03E-02 | 3.76E-05 | 1.80E-05 | 2.95E-03 |
| 2.90E-06 | 120 | 0.005 | 2.38E-03 | 7.01E-02 | 3.99E-05 | 1.88E-05 | 3.27E-03 |
| 2.90E-06 | 125 | 0.005 | 2.23E-03 | 7.14E-02 | 4.04E-05 | 1.92E-05 | 3.40E-03 |
| 2.90E-06 | 110 | 0.01 | 1.97E-03 | 8.87E-02 | 5.86E-05 | 2.84E-05 | 1.26E-02 |
| 2.90E-06 | 115 | 0.01 | 1.81E-03 | 8.67E-02 | 6.00E-05 | 2.94E-05 | 1.11E-02 |
| 2.90E-06 | 120 | 0.01 | 1.75E-03 | 8.42E-02 | 5.88E-05 | 2.90E-05 | 1.07E-02 |
| 2.90E-06 | 125 | 0.01 | 1.72E-03 | 8.02E-02 | 5.68E-05 | 2.82E-05 | 1.07E-02 |

the relaxation time, $\lambda$. From experiments, we know that relaxation times decrease as the temperature increases. If we assume that $H_c = \lambda\,\dot{\gamma}_c$ is a dimensionless constant at the critical shear rate at different temperatures, then the critical shear rate, $\dot{\gamma}_c$, increases as relaxation time, $\lambda$, decreases. Since the viscosity minimum is associated with the physics of supermolecular structuring, it is evident that an increase in temperature acts to reduce the degree of structuring by increasing the kinetic energy of the polymer chain segments. In order to offset this reduction, a larger deformation rate is required.

Also in Figure 3, we observe that the critical shear rate decreases with increasing polymer concentration. We can explain this relationship by considering that, as the polymer concentration increases, the effect of the polymer is magnified. In a previous article,[1] we provided evidence that shear-thickening behavior is due to the decrease in size and anisotropy of the associations of polymer particles in the solvent. The sizes of these polymer structures presumably increase with polymer concentration. Consequently, it is plausible that the rate of size decrease also accelerates with polymer concentration, and so the minimum shear rate required for this size decrease to manifest itself is correspondingly smaller. Furthermore, since $\lambda$ increases with polymer concentration, a smaller value of $\dot{\gamma}_c$ is required to attain the critical value of $H_c$.

In Figure 4, we plot $\dot{\gamma}_c$ values of PS/d solutions as a function of polymer concentration for five different molecular weights. Figure 4 supports the conclusion taken from Figure 3 that, as polymer concentration is increased, the critical shear rate decreases for all molecular weights. The scatter in the data is generated from two sources of error, primarily experimental error from the original work[12] and, to a lesser extent, error due to the computer software used to read precise numerical values from the published plots.

Additionally in Figure 4, we see that the critical shear rate generally decreases with increasing molecular weight. At the two highest values of molecular weight, we see a partial violation of this explanation of molecular weight dependence. We can explain this violation by postulating that at very high molecular weights, we reach a plateau where the critical shear rate is no longer a function of molecular weight. Such a plateau exists because the effect of increasing chain length will become weaker when the molecular weight is already very high. Additionally, the distribution of molecular weight will influence the effect of molecular weight on critical shear rate. However, we do not know the distribution of molecular weight for these polymers and cannot evaluate this effect. Furthermore, since $\lambda$ generally increases with molecular weight, again the dimensionless quantity $H_c$ accurately describes the qualitative solution behavior.

In Figure 5, we plot the critical shear rates of PE/x solutions as functions of temperature for two molecular weights. Figure 5 supports the conclusion from Figure 4 that the critical shear rate decreases with increasing molecular weight and the conclusion from Figure 3 that the critical shear rate increases with increasing temperature for all concentrations. However, for the lower molecular weight value, $\dot{\gamma}_c$ decreases slightly with increasing temperature. We suspect that this slight, anomalous trend is within the experimental error of the data.

## Data Fitting Methodology

The method we used to optimize our parameters $\lambda_1$, $\lambda_2$, $n_1$, $n_2$, and $\theta$ in the TCMM Model was Nelder and Mead's Downhill Simplex Method,[19] which requires only functional evaluations, not derivatives. While this method is not very efficient in terms of the num-

ber of function evaluations it requires, the simplex method can always find a minimum, provided that one exists. However, the Simplex Method is not guaranteed to find a global minimum. On the contrary, the minimum found is strongly dependent on the initial guess of the problem. To compensate for this shortcoming, we scattered our initial guesses in the five-dimensional parameter space to find the deepest minimum. If we were dealing with a series of data sets where, for example, only molecular weight was varied, then we used the scatter technique to find the minimum for the first data set. For each subsequent data set in the series, we used the optimized parameter set from the previous data set in the series as the initial guess.

Within the Simplex Method, the evolution expressions for the conformation tensors, eq. (3), were solved using an iterative Newton-Raphson Method for the current set of parameter values. The extra stress tensor expression, eq. (4), was then evaluated, and the shear viscosity calculated. This gave rise to an objective function, defined below, which the Simplex Method tried to minimize.

Because we were interested in modeling the shear-thickening phenomenon, we fitted our parameters primarily to experimental data in the shear-thickening range of shear rates. This range is bounded by $\dot{\gamma}_c$ and $\dot{\gamma}_m$ (see Fig. 1). We used the following expression for our objective function, $F^{\eta}_{\text{obj}}$, which is the function minimized by the Simplex Method:

$$F^{\eta}_{obj} = \left[ \frac{\sum_{i=1}^{n^{\eta}_{data}} w_i \left( \frac{\eta_i^e - \eta_i^m}{\eta_i^e} \right)^2 + w(\eta(\dot{\gamma}_c)) \left( \frac{\eta(\dot{\gamma}_c)^e - \eta(\dot{\gamma}_c)^m}{\eta(\dot{\gamma}_c)^e} \right)^2 + w(\dot{\gamma}_c) \left( \frac{\dot{\gamma}_c^e - \dot{\gamma}_c^m}{\dot{\gamma}_c^e} \right)^2}{n^{\eta}_{data} + 2} \right]^{1/2}, \quad (15)$$

where $w(\eta(\dot{\gamma}_c))$ is the weighting factor for the value of the viscosity at the critical shear rate, $w(\dot{\gamma}_c)$ is the weighting factor for the value of $\dot{\gamma}_c$, $n^{\eta}_{\text{data}}$ is the number of experimental viscosity data points, $\eta_i^e$ is the $i$-th experimental viscosity data point, and $\eta_i^m$ is the corresponding value as calculated with the TCMM Model. We set $w(\eta(\dot{\gamma})_c)$ and $w(\dot{\gamma}_c)$ equal to 100 in order to be sure that we fit the experimental value of the viscosity well at $\dot{\gamma}_c$. The weighting factor for all other data points was given by

$$w_i = \begin{cases} 0 & \dot{\gamma} < \dot{\gamma}_c^e \\ 1 & \dot{\gamma}_c^e < \dot{\gamma} < \dot{\gamma}_m^e \\ 0 & \dot{\gamma} > \dot{\gamma}_m^e \end{cases}. \quad (16)$$

In some cases, we had available experimental data for the dichroism. When this was the case, we slightly altered the optimization procedure, described above, by adding a sixth fitting parameter, $\langle \mathbf{aa} \rangle_0$, which characterized the size of the supermolecular structures. [This parameter appears in the expression for the linear dichroism, eq. (6).] The same numerical methods were used to optimize all six parameters; however, a new objective function was needed for the dichroism data:

$$F^{d}_{obj} = \left[ \frac{\sum_{i=1}^{n^{d}_{data}} w_i \left( \frac{\Delta n_i''^e - \Delta n_i''^m}{\Delta n''^e_{\max}} \right)^2}{n^{d}_{data}} \right]^{1/2}, \quad (17)$$

where $w_i = 1$, is the weighting factor for the dichroism, $\Delta n_i''^e$ is the experimental dichroism data taken from the literature,[2,3] $\Delta n_i''^m$ is the value computed by the TCCM Model, and $\Delta n_{\max}''^e$ is the experimental value of the dichroism at $\dot{\gamma}_d$.

We used two different methods to optimize the six parameters, $\lambda_1$, $\lambda_2$, $n_1$, $n_2$, $\theta$, and $\langle \mathbf{aa} \rangle_0$, for the cases where dichroism data were available. One method was to use the optimized values for the five parameters $\lambda_1$, $\lambda_2$, $n_1$, $n_2$, and $\theta$ using only the viscosity data and subsequently optimizing to the dichroism data varying only the sixth parameter. The second method was to optimize all six parameters simultaneously to a new objective function, $F_{\text{obj}} = F^{\eta}_{\text{obj}} + F_{\text{obj}}{}^{d}$. We compare the two methods of optimization in the following section.

## RESULTS AND DISCUSSION

Three different experimental studies provided the data for our comparisons. These were the capillary viscometric examinations of Layec-Raphalen and Wolff[12] and Vrahopoulou and McHugh,[13,18] and the Couette rheo-optical experiments of Kishbaugh and McHugh.[2,3] All experimental data presented in the above sources were parameterized using the TCMM Model. Parameter values for a sampling of these experiments are presented in Tables I and II, as well as in the following figures.

### A comparison of the General Trends of the Theoretical and Experimental Results

In Figure 6, we show some typical optimized fits of the TCMM Model for PE/x solutions ($M = 2.90 \times 10^6$ g/mole, $c = 0.05$ wt %) with the experimental data of Vrahopoulou and McHugh.[13,18] The TCCM Model

**TABLE II**
**Optimized parameters for PS/d Solutions of Layec-Raphalen and Wolff[12]**

| $M$ (g/mole) | $c$ (g/dL) | $\lambda_1$ (s) | $\lambda_2$ (s) | $n_1$ (mole/m$^3$) | $n_2$ (mole/m$^3$) | $\theta$ (−) |
|---|---|---|---|---|---|---|
| 8.40E-06 | 0.167 | 1.28E-02 | 4.17E-02 | 1.95E-04 | 2.00E-06 | 2.82E-03 |
| 8.40E-06 | 0.110 | 8.82E-03 | 2.91E-02 | 2.49E-04 | 3.82E-06 | 2.40E-03 |
| 8.40E-06 | 0.0889 | 1.16E-02 | 6.25E-02 | 1.41E-04 | 2.76E-05 | 2.58E-04 |
| 8.40E-06 | 0.0675 | 1.18E-02 | 6.14E-02 | 1.33E-04 | 2.60E-05 | 2.58E-04 |
| 8.40E-06 | 0.0557 | 1.07E-02 | 5.85E-02 | 1.39E-04 | 3.05E-05 | 2.59E-04 |
| 8.40E-06 | 0.0446 | 1.07E-02 | 6.02E-02 | 1.33E-04 | 3.17E-05 | 1.73E-04 |
| 8.40E-06 | 0.0326 | 1.07E-02 | 6.03E-02 | 1.29E-04 | 3.25E-05 | 1.78E-04 |
| 8.40E-06 | 0.0245 | 8.04E-03 | 4.56E-02 | 1.68E-04 | 4.29E-05 | 2.70E-04 |
| 7.32E-06 | 0.129 | 1.63E-02 | 1.25E-01 | 9.74E-05 | 2.76E-05 | 2.52E-04 |
| 7.32E-06 | 0.109 | 1.47E-02 | 1.47E-01 | 9.72E-05 | 3.19E-05 | 1.74E-04 |
| 7.32E-06 | 0.091 | 1.12E-02 | 1.39E-01 | 1.19E-04 | 4.26E-05 | 1.84E-04 |
| 7.32E-06 | 0.0642 | 1.20E-02 | 9.24E-02 | 1.15E-04 | 3.33E-05 | 1.68E-04 |
| 7.32E-06 | 0.0505 | 4.84E-03 | 4.48E-01 | 2.16E-04 | 1.07E-04 | 2.35E-04 |
| 7.32E-06 | 0.0428 | 4.83E-03 | 4.54E-01 | 2.12E-04 | 1.09E-04 | 3.28E-04 |
| 7.32E-06 | 0.0326 | 4.41E-03 | 2.90E-01 | 2.28E-04 | 1.17E-04 | 2.82E-04 |
| 7.32E-06 | 0.0251 | 4.69E-03 | 2.62E-01 | 2.11E-04 | 1.10E-04 | 3.83E-04 |
| 7.32E-06 | 0.0192 | 4.78E-03 | 1.89E-01 | 2.07E-04 | 1.06E-04 | 3.40E-04 |
| 3.70E-06 | 0.2450 | 9.72E-03 | 2.93E-02 | 2.89E-04 | 2.34E-06 | 2.12E-03 |
| 3.70E-06 | 0.195 | 8.07E-03 | 2.49E-02 | 3.09E-04 | 2.82E-06 | 3.27E-03 |
| 3.70E-06 | 0.149 | 1.07E-02 | 5.97E-02 | 1.59E-04 | 3.82E-05 | 9.26E-05 |
| 3.70E-06 | 0.108 | 9.48E-03 | 4.89E-02 | 1.72E-04 | 3.68E-05 | 1.25E-04 |
| 3.70E-06 | 0.0831 | 6.10E-03 | 4.54E-02 | 2.24E-04 | 7.34E-05 | 1.30E-04 |
| 3.70E-06 | 0.0653 | 5.89E-03 | 6.43E-02 | 2.06E-04 | 8.28E-05 | 1.10E-04 |
| 3.70E-06 | 0.0472 | 3.73E-03 | 1.01E-01 | 2.82E-04 | 1.40E-04 | 1.50E-04 |
| 3.37E-06 | 0.297 | 5.71E-03 | 1.75E-02 | 4.80E-04 | 4.61E-06 | 3.37E-03 |
| 3.37E-06 | 0.235 | 5.68E-03 | 1.77E-02 | 4.38E-04 | 5.75E-06 | 2.74E-03 |
| 3.37E-06 | 0.177 | 4.21E-03 | 1.31E-02 | 5.39E-04 | 6.38E-06 | 2.88E-03 |
| 3.37E-06 | 0.132 | 3.23E-03 | 9.86E-03 | 7.06E-04 | 4.91E-06 | 3.97E-03 |
| 3.37E-06 | 0.0888 | 6.35E-03 | 4.54E-02 | 2.13E-04 | 6.78E-05 | 1.29E-04 |
| 3.37E-06 | 0.0514 | 3.27E-03 | 7.76E-02 | 3.22E-04 | 1.57E-04 | 1.42E-04 |
| 3.37E-06 | 0.0448 | 2.84E-03 | 7.71E-02 | 3.63E-04 | 1.80E-04 | 1.23E-04 |
| 2.74E-06 | 0.401 | 4.90E-03 | 1.48E-02 | 6.24E-04 | 1.18E-06 | 3.54E-03 |
| 2.74E-06 | 0.241 | 5.24E-03 | 1.57E-02 | 4.74E-04 | 1.13E-06 | 1.90E-03 |
| 2.74E-06 | 0.197 | 4.32E-03 | 1.30E-02 | 5.41E-04 | 1.67E-06 | 1.67E-03 |
| 2.74E-06 | 0.161 | 4.29E-03 | 1.29E-02 | 5.18E-04 | 1.98E-06 | 1.50E-03 |

faithfully demonstrates the critical features of the experimental data. At a given temperature, both the model and experimental reduced viscosity display a minimum (at $\dot{\gamma}_c$) and a maximum (near $\dot{\gamma}_m$) with respect to shear rate. Moreover, the TCMM Model also quantifies the temperature dependence of the viscosity correctly. The viscosity decreases with increasing temperature at any particular shear rate, and the minima of the viscosity curves occur at increasing values of $\dot{\gamma}_c$ as the temperature increases. Therefore, the overall performance of the TCMM Model is quite satisfactory, especially in the shear-thickening range of shear rates where the parameter fitting was concentrated.

The TCMM Model has several typical discrepancies with the experimental data. First, at low shear rates, the TCMM Model always overpredicts the viscosity. Second, after the value of the shear rate where the maximum viscosity is observed, $\dot{\gamma}_m$, the TCMM Model does not predict as steep a drop in the viscosity as is observed experimentally. We could improve the fit in these two shear-rate regions by incorporating more complicated features into the model, such as shear-rate dependent relaxation times. However, these additional features would provide only quantitative improvement in shear-rate regions outside of the main region of interest at the cost of requiring additional parameters and without necessarily providing any new, relevant physical information.

### The Dependence of $\lambda_1$ on Temperature, Concentration, and Molecular Weight

In Figure 7, we plot the relaxation time of the chain conformation mode, $\lambda_1$, as a function of temperature for five PE/x solutions of different molecular weights and concentrations. We see that $\lambda_1$ decreases with increasing temperature in all cases. As the temperature increases, the kinetic motion of the individual atoms increases, which makes polymer chain conformational rearrangements easier.

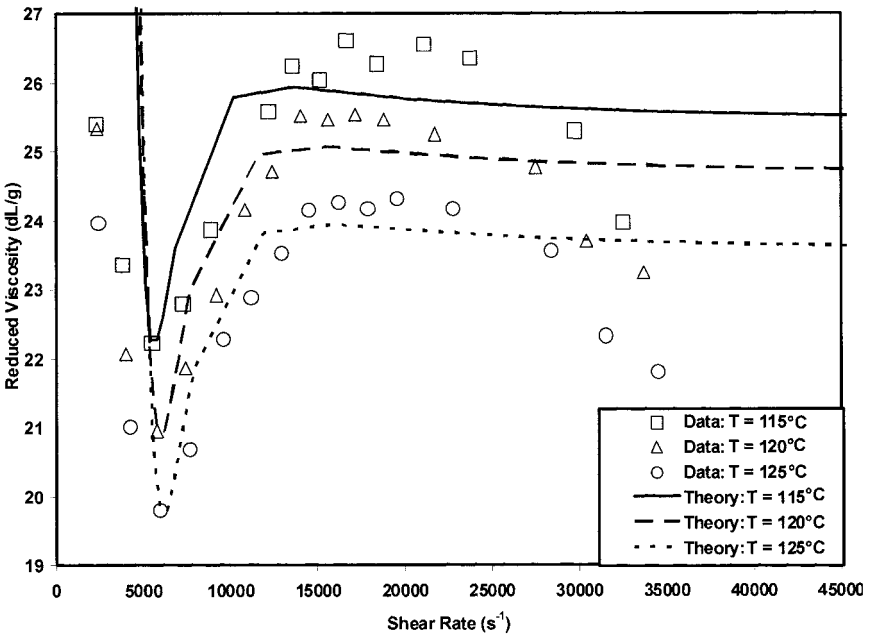


**Figure 6** A typical plot of viscosity versus shear rate comparing model fits and experimental data for a PE/x solution at various temperatures.

Also in Figure 7, we observe that, at constant temperature and molecular weight ($2.90 \times 10^6$ g/mole), there appears to be a non-monotonic dependence between $\lambda_1$ and polymer concentration. Figure 8 contains additional information about the functional dependence of this relaxation time on polymer concentration. In this figure, we plot the relaxation time as a function of concentration for five different molecular weights of PS/d solutions at 25°C. The relaxation time generally increases with increasing concentration at a constant molecular weight, but it seems to arrive at a plateau when the polymer concentration reaches 0.25 g/dL. We can explain the increase in $\lambda_1$ at low concentrations by considering that, as the polymer concentration increases, the extent of intermolecular interactions increases, thus making it more difficult for the polymer chains to relax. We also observe a plateau at higher polymer concentrations, which is possibly caused by the increased number of polymer chains that take part in the supermolecular structuring: larger and more numerous structures require more polymer chains, thus decreasing the number of free polymer chains remaining in solution.

We can also consider the dependence of $\lambda_1$ on molecular weight at constant temperature and polymer concentration. Figure 8 shows that $\lambda_1$ generally increases with increasing molecular weight for the same temperature and polymer concentration. As the average length of the polymer chain increases, it becomes more difficult for the molecule to relax. Therefore, an increase in relaxation time with increasing molecular weight is expected. However, at the highest molecular weights, there are exceptions to this trend. This anomalous dependence at high molecular weights is also observed in the values of the critical shear rates obtained from the experimental data (see Fig. 4). In all likelihood, at some point further increases in molecular weight probably have negligible effect upon the phenomenon under consideration.

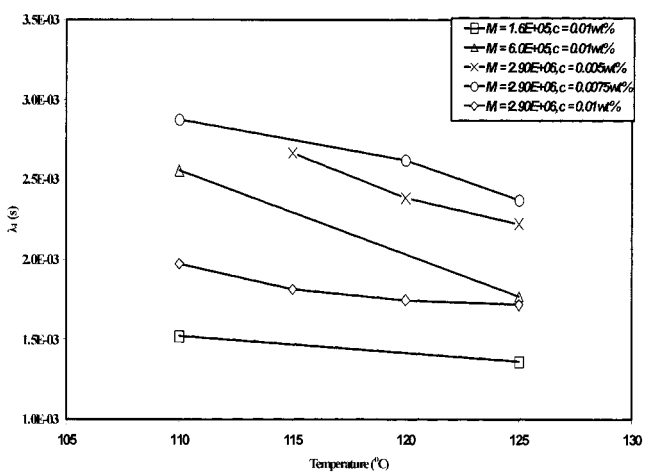


**Figure 7** The parameter $\lambda_1$ as a function of temperature for PE/x solutions of different molecular weights and concentrations.

## The Dependence of $\lambda_2$ on Temperature, Concentration, and Molecular Weight

In Figure 9, we plot the relaxation time of the structure conformation mode, $\lambda_2$, as a function of temperature for five cases of PE/x solutions of different molecular

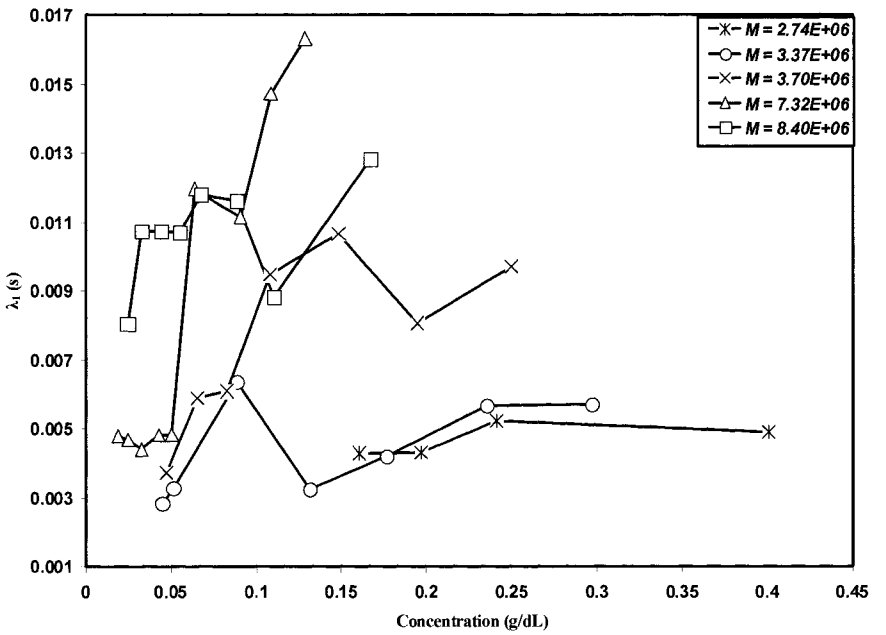


**Figure 8** The parameter $\lambda_1$ as a function of concentration for PS/d solutions of different molecular weights.

weights and concentrations. We see that $\lambda_2$ decreases with increasing temperature in most cases. This trend is similar to the $\lambda_1$ temperature trend for the same reason; namely, the supermolecular structures relax more easily at higher temperatures.

Also in Figure 9, we observe, at constant temperature and molecular weight ($2.90 \times 10^6$ g/mole), an increase in $\lambda_2$ with polymer concentration, in contrast to the behavior of $\lambda_1$, which shows a maximum. In Figure 10, we plot $\lambda_2$ against concentration for five different molecular weights of PS/d solutions at 25°C. We see that this relaxation time increases when concentration is lower than about 0.05 g/dL, and then decreases with increasing concentration until it reaches a plateau at about 0.25 g/dL. To rationalize such behavior, one must resort to evidence from the previous article[1]: the size of the structures does not necessarily scale with concentration. It is quite possible that the structures are fewer and larger at lower concentrations and smaller but more numerous at higher concentrations.

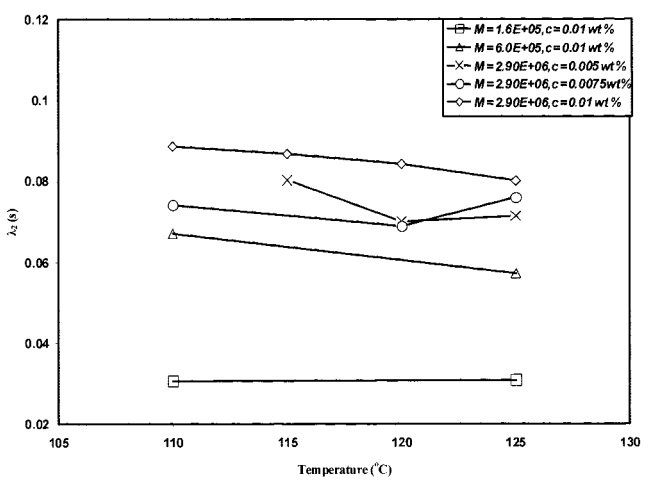


**Figure 9** The parameter $\lambda_2$ as a function of temperature for PE/x solutions of different molecular weights and concentrations.

We can also consider the dependence of $\lambda_2$ on molecular weight at constant temperature and polymer concentration. In Figure 9, we see that $\lambda_2$ increases with molecular weight. Figure 10 shows the same general trend, except at the highest molecular weight, as was the case with $\lambda_1$. This probably occurs for the same reason; namely, that it is more difficult for the longer polymer chains, which make up the supermolecular structures, to relax.

### The Dependence of $n_1$ on Temperature, Concentration, and Molecular Weight

In Figure 11, we plot the effective concentration of the chain conformation mode, $n_1$, as a function of temperature for five cases of PE/x solutions of different molecular weights and concentrations. Figure 11 shows that $n_1$ is generally insensitive to temperature changes between 110°C and 125°C. The average percentage change in $n_1$ with temperature is less than 10%. We expect little change in $n_1$ with temperature, as temperature should not have any effect on the amount of mass in the solutions. However, it does have a slight effect for concentrations that are measured in weight percents, since the solvent density depends on tem-

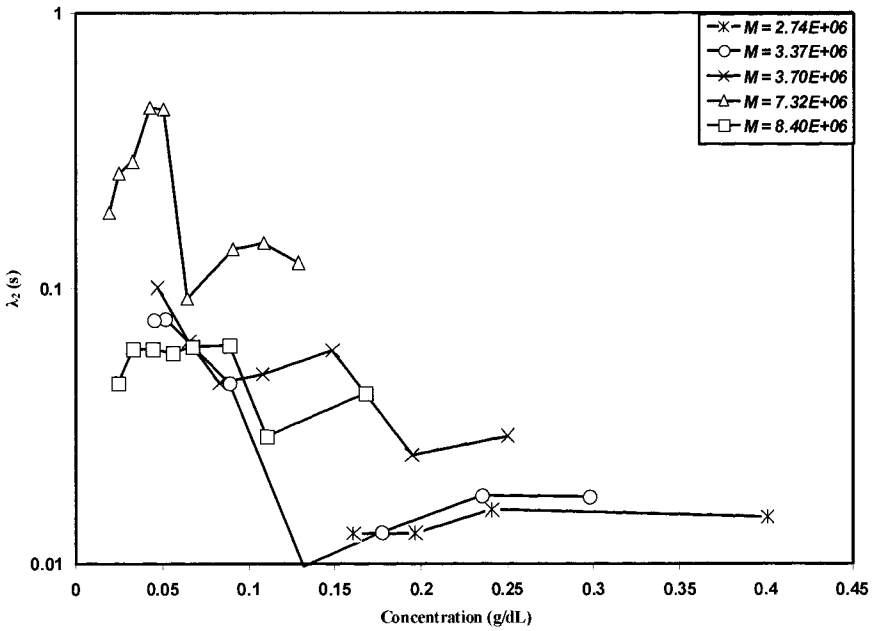


**Figure 10** The parameter $\lambda_2$ as a function of concentration for PS/d solutions of different molecular weights.

perature: as the temperature increases, the solvent density decreases, and thus the effective mass of polymer in a unit volume of solvent decreases as well. These variations are generally within about 10%.

In Figure 12, we plot the effective concentration of the chain mode as a function of concentration for five different molecular weights of PS/d solutions at 25°C. This figure demonstrates that $n_1$ generally increases with increasing concentration at constant molecular weight, as expected: the increasing polymer concentration certainly increases the effective concentration of the free chains in solution.

We can also consider the dependence of $n_1$ on molecular weight at constant temperature and polymer concentration. Results here are inconclusive.

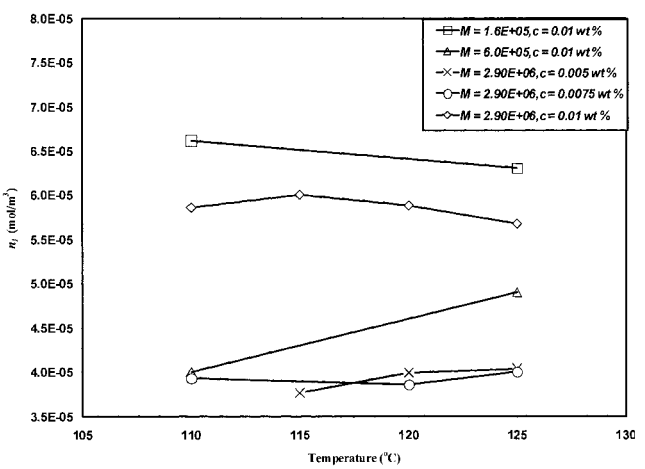


**Figure 11** The parameter $n_1$ as a function of temperature for PE/x solutions of different molecular weights and concentrations.

This can probably be ascribed to experimental data scatter and uncertainty in the five-parameter optimization.

### The Dependence of $n_2$ on Temperature, Concentration, and Molecular Weight

Figure 13 plots the effective concentration of the structure mode, $n_2$, as a function of temperature for five cases of PE/x solutions of different molecular weights and concentrations. Figure 13 demonstrates that $n_2$ is also generally insensitive to temperature changes between 110°C and 125°C.

In Figure 14, we plot $n_2$ as a function of concentration for five different molecular weights of PS/d at 25°C. We observe the general trend that $n_2$ decreases with increasing polymer concentration. Such an observation is consistent with the results presented in ref. 1, wherein it is noted that structure size increases with increasing polymer concentration. However, as the structure size increased, the number of structures decreased. Hence, $n_2$ decreased with increasing polymer concentration.

Figure 14 also demonstrates that $n_2$ generally decreases with increasing molecular weight for the same polymer concentration. The rationale for this trend is as above: increasing the molecular weight produces larger, but fewer, structures.

### Dependence of $\theta$ on Temperature, Concentration, and Molecular Weight

In Figure 15, we plot the coupling parameter, $\theta$, as a function of temperature for five samples of PE/x so-

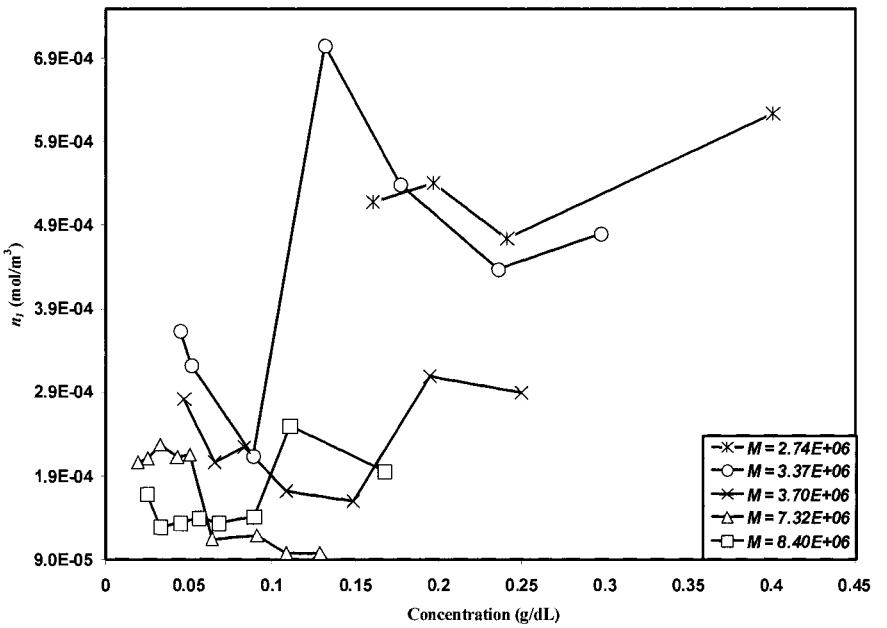


**Figure 12** The parameter $n_1$ as a function of concentration for PS/d solutions of different molecular weights.

lutions of different molecular weights and concentrations. This figure shows that $\theta$ is generally insensitive to temperature changes, as was shown previously.[1]

In Figure 16, we plot the coupling parameter as a function of concentration for five different molecular weight samples of PS/d solutions at 25°C. This figure shows that $\theta$ is essentially independent of concentration at lower concentrations, but that it generally increases with increasing concentration at higher concentrations. In order to rationalize this behavior, we consider that $n_1$ generally increases with increasing concentration and that $n_2$ generally decreases. The coupling parameter is most likely a function of both $n_1$ and $n_2$; a molecular model corresponding to the macroscopic TCMM Model might reveal an exact functional dependency.

We can also consider the dependence of $\theta$ on molecular weight at constant temperature and polymer concentration. Figure 15 shows that $\theta$ increases with increasing molecular weight. Figure 16 also shows that $\theta$ generally increases with increasing molecular weight for the same polymer concentration. As the polymer chains become longer with increasing molecular weight, it seems reasonable that a greater degree of interaction between the modes would develop. Note that, in all cases, the coupling parameter is a small, positive fraction, which is consistent with previous examinations of the TCMM Model.[16]

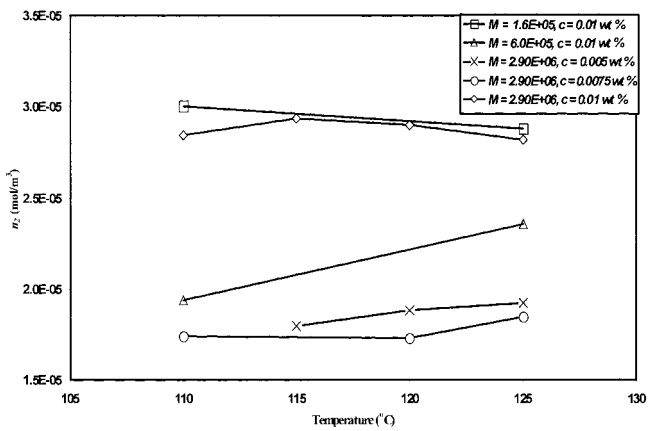


**Figure 13** The parameter $n_2$ as a function of temperature for PE/x solutions of different molecular weights and concentrations.

## Inclusion of Dichroism Data in Parameter Fitting

For some of the experimental runs, we have available measurements of both the shear viscosity and the dichroism at steady state. As noted before, the dichroism calculation with the TCMM Model requires one additional parameter beyond the five needed for fitting the viscosity data only. We optimized the additional data using two methods, as described in the preceding section. In Method 5+1, we optimized the first five parameters to the viscosity data only. Then, holding these parameters constant, we optimized the sixth parameter, $\langle \mathbf{aa} \rangle_0$, individually to the dichroism data. In Method 6, we simultaneously optimized all six parameters to the combined objective function, $F_{\text{obj}} = F_{\text{obj}}^{\eta} + F_{\text{obj}}^{d}$, incorporating both viscosity and dichroism data.

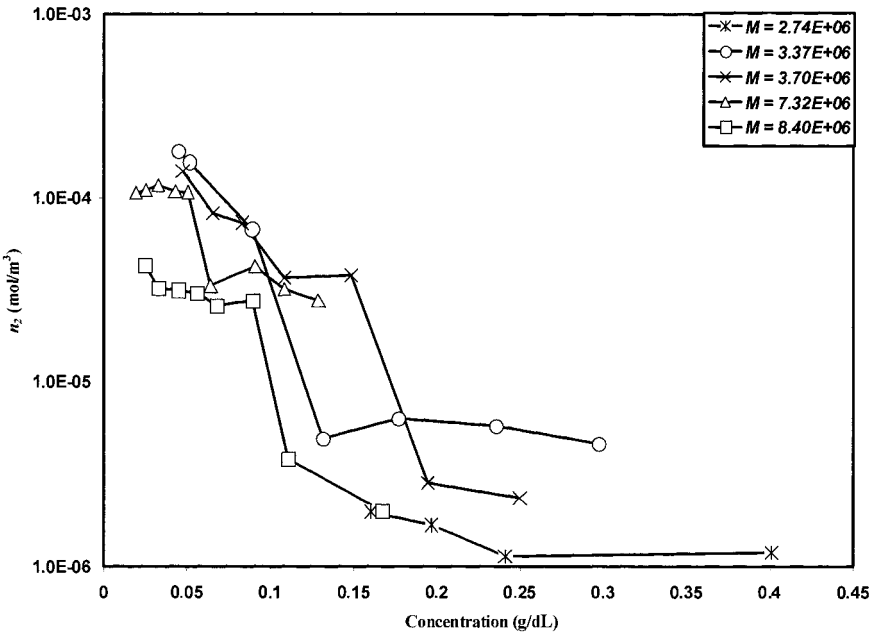


**Figure 14** The parameter $n_2$ as a function of concentration for PS/d solutions of different molecular weights.

In Figure 17, we plot the viscosity and dichroism as functions of the shear rate for a PS/d solution ($6.8 \times 10^6$ g/mole, $T = 25$°C, and $c = 0.25$g/dL). As in Figure 2, we observe a maximum in the dichroism curve that occurs shortly before the minimum in the viscosity curve. Figure 17 demonstrates that the TCMM Model can fit the experimental data for viscosity and dichroism simultaneously, and that similar results can be obtained using either of the two different methods of optimization. Consequently, a sufficiently good fit of the TCMM Model to the experimental data requires only viscosity data. Very little improvement, if any, is obtained by optimizing to additional dichroism data. We should also point out that, if we ignore the viscosity data and fit all six parameters to the dichroism data only, then we can fit the experimental dichroism data well but the viscosity fittings are qualitatively and quantitatively incorrect. Thus dichroism data alone is insufficient to obtain a decent fit of the TCMM Model.

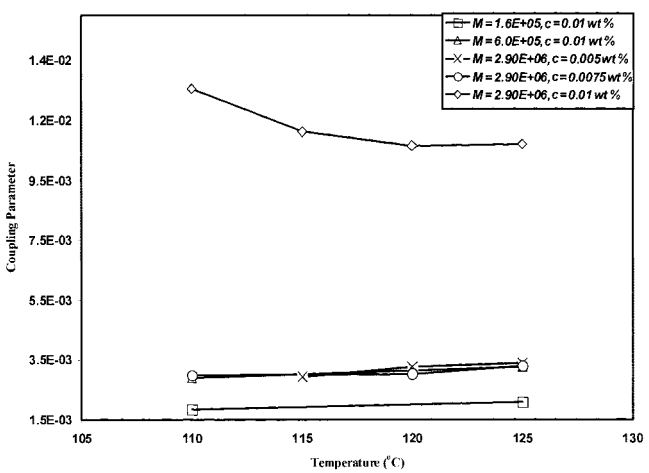


**Figure 15** The paramter $\theta$ as a function of temperature for PE/x solutions of different molecular weights and concentrations.

In Figure 18, we show the behavior of the parameter $\langle \mathbf{aa} \rangle_0$ as a function of polymer concentration for the solutions where dichroism data was available. The variations of this structure-size parameter with concentration is in both directions; in general, it varies inversely with the number of structures formed in the solutions. It appears that $\langle \mathbf{aa} \rangle_0$ does not depend greatly on molecular weight, indicating that the typical structure size does not vary much from one polymer sample to another.

## CONCLUSIONS

In this work, we have fit the TCMM Model to experimental data for viscosity and dichroism during steady-state shear flow. The TCMM Model can account for the qualitative features of both the viscosity and the dichroism data. We fit the six parameters (two relaxation times, two modal concentrations, a coupling parameter, and a particle size parameter) of the TCMM Model in order to obtain quantitative agreement with the experimental data.

From this fitting procedure, we were able to establish the functional dependence of the relaxation times, modal concentrations, coupling parameter,

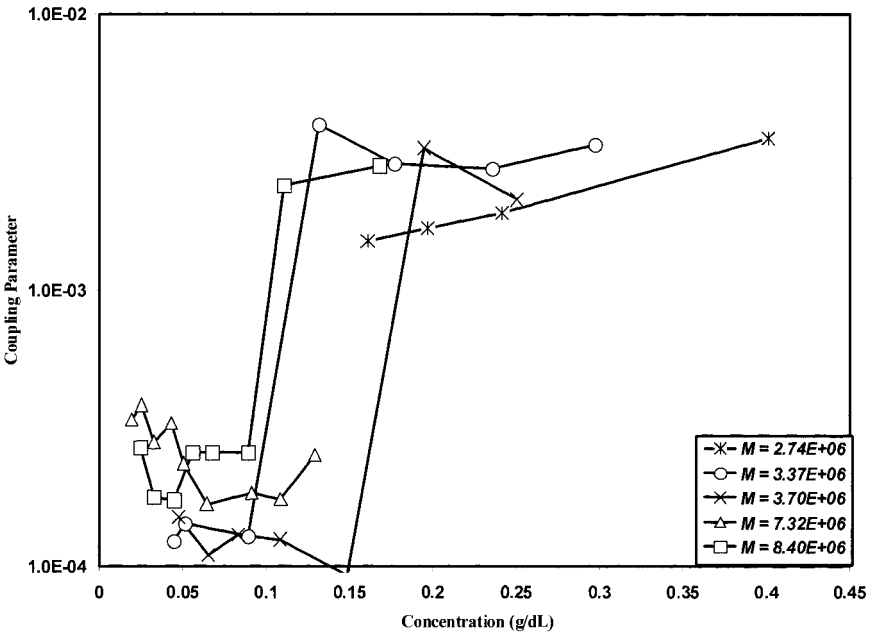


**Figure 16** The parameter $\theta$ as a function of concentration for PS/d solutions of different molecular weights.

and particle size parameter as functions of temperature, polymer concentration, and polymer molecular weight, using the physical basis of the TCMM Model. We showed that, by optimizing to only the viscosity data, we were able to obtain the same relaxation times, modal concentrations, and coupling parameter as when optimizing to both the viscosity and dichroism data simultaneously. This is useful because, typically, the dichroism data is not available.

Thus the TCMM Model seems to give an adequate quantitative description of the shear-thickening phenomenon, and to offer new insight into the physics of structure formation in dilute polymer solutions, as first discussed in ref. 1. Further validation of the model may be obtained by examining transient experimental data taken during start up and cessation of shear flow.[20]

The authors would like to acknowledge graduate student support from the Department of Chemical Engineering at The University of Tennessee. Additionally, the authors would like to thank P.A. Kamerkar and C.W. Reneau for their insightful discussions during the preparation of this manuscript.

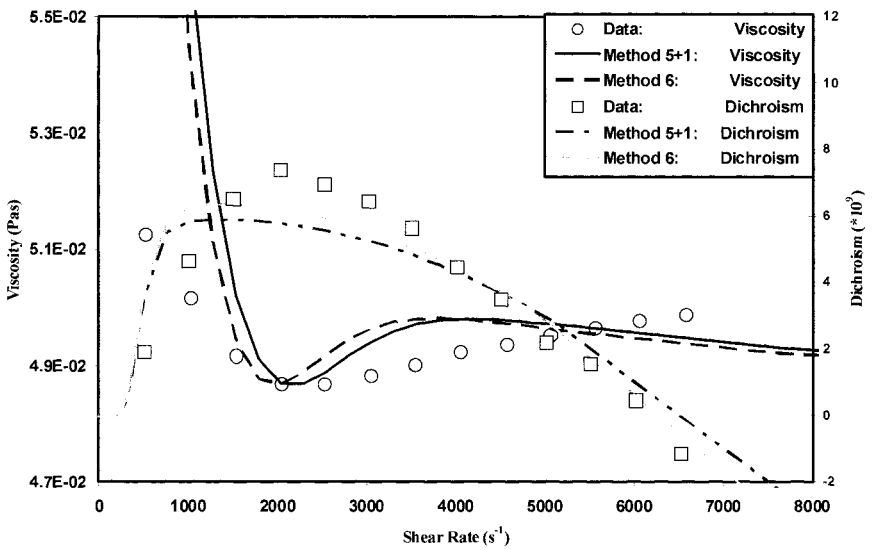


**Figure 17** Viscosity and dichroism versus shear rate for the TCMM Model and experimental data for a PS/d solution ($6.8 \times 10^6$ g/mole, $c = 0.25$ g/dL) at 25°C.

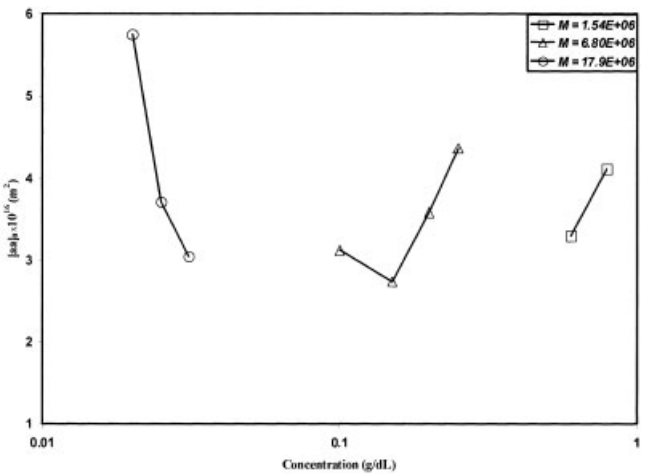


**Figure 18** The parameter $\langle \mathbf{aa} \rangle_0$ as a function of concentration for PS/d solutions of different molecular weights.

## References


1. Edwards, B. J.; Keffer, D. J.; Reneau, C. W. J Appl Polym Sci 2002, 85, 1714.
2. Kishbaugh, A. J. Ph.D. Dissertation, University of Illinois, 1992.
3. Kishbaugh, A. J.; McHugh, A. J. Rheol Acta 1993, 32, 9.
4. Bird, R. B.; Curtiss, C. F.; Armstrong, R. C.; Hassager, O. Dynamics of Polymeric Fluids, 2nd ed.; John Wiley & Sons: New York, 1987; Vols. 1 and 2.
5. Peterlin, A. J Chem Phys 1960, 33, 1799.
6. Peterlin, A. Makromol Chem 1961, 45, 338.
7. Kishbaugh, A. J.; McHugh, A. J. J Non-Newtonian Fluid Mech 1990, 34, 181.
8. Wolff, C.; Silberberg, A.; Priel, Z.; Layec-Raphalen, M. N. Polymer 1979, 20, 281.
9. Wolff, C. Adv Colloid Interface Sci 1982, 17, 263.
10. Vrahopoulou, E. P.; McHugh, A. J. J Rheol 1987, 31, 371.
11. Vrahopoulou, E. P.; McHugh, A. J. Chem Eng Commun 1987, 57, 289.
12. Layec-Raphalen, M.; Wolff, C. J Non-Newtonian Fluid Mech 1976, 1, 159.
13. Vrahopoulou, E. P.; McHugh, A. J. J Non-Newtonian Fluid Mech 1987, 25, 157.
14. Kishbaugh, A. J.; McHugh, A. J. Rheol Acta 1993, 32, 115.
15. Beris, A. N.; Edwards, B. J. Thermodynamics of Flowing Systems; Oxford University Press: New York, 1994.
16. Edwards, B. J.; Beris, A. N.; Mavrantzas, V. G. J Rheol 1996, 40, 917.
17. Rodger, A.; Nordėnd, B. Circular Dichroism and Linear Dichroism; Oxford University Press: New York, 1997.
18. Vrahopoulou, E. P. Ph.D. Dissertation, University of Illinois, 1986.
19. Press, W. H.; Vettuling, W. T.; Tevkolsky, S. A.; Flannery, B. P. Numerical Recipes in Fortran 77; Cambridge University Press: Cambridge, 1992.
20. Kamerkar, P. A.; Edwards, B. J.; Keffer, D. J.; Reneau, C. W. Chem Eng Commun, to press.